

NORTHEASTERN UNIVERSITY

UNDERGRADUATE THESIS

---

**An Improved Method for Real-Time  
Ratiometric Quantitative Fluorescent  
Microscopy in the Pharynx of *C. elegans***

---

*Author:*  
Sean Johnsen

*Supervisor:*  
Dr. Javier Apfeld

*A thesis submitted in fulfillment of the requirements  
for the degree of Bachelor of Science  
in the*

**Department of Biology**

April 21, 2019

*“...the grandest discoveries of science have been but the rewards of accurate measurement and patient long-continued labour in the minute sifting of numerical results.”*

Lord Kelvin

NORTHEASTERN UNIVERSITY

## *Abstract*

Faculty Name  
Department of Biology

Bachelor of Science

### **An Improved Method for Real-Time Ratiometric Quantitative Fluorescent Microscopy in the Pharynx of *C. elegans***

by Sean Johnsen

Genetically-encoded redox-sensitive biosensors (roGFPs) enable real-time visualization of protein oxidation with subcellular resolution in live animals. Oxidation reversibly changes the excitation spectrum of roGFPs, and we can calculate the proportion of oxidized sensors by fluorescence ratio microscopy. Ratios are obtained from a sequence of two images taken with different illumination (410 and 470 nm). Accurate calculation of protein oxidation requires precise ratio measurement.

In our previous work we developed a semi-automated imaging pipeline that measures fluorescence ratios along the centerline that traces the anterior-posterior axis of the pharynx, the worm's feeding organ. This pipeline is labor intensive because it requires a manual step to ensure there is no movement between images. Here we present an improved image analysis pipeline for biosensor imaging of the feeding muscles *C. elegans*.

For our new pipeline, we set out to improve centerline quality and reduce the measurement error introduced by even slight movement between images. We improved centerline quality by detecting the edges of the pharynx with a Sobel-operator thresholding algorithm that performs well even in the presence of gut autofluorescence, and by using a new spline-fitting algorithm that also incorporates the overall shape of the worm from a transmitted light image. To reduce errors due to movement we now draw centerlines in each image of the pharynx, instead of just one. We also match the position of points along each centerline with a functional data analysis-based version of dynamic time warping that performs well even for complex movements between images. In practice, the new pipeline requires minimal manual intervention and improves the precision of fluorescence ratio measurements along the anterior-posterior axis of the pharynx.

## *Acknowledgements*

I would like to express my sincere gratitude to all of those people who have supported and encouraged me, but especially to... My advisor, Professor Javier Apfeld, for his unending guidance, enthusiasm, support, and edification; Jodie Norris, for guiding me through lab work - I would have been utterly lost but for her patient and kind assistance; Julian Stanley, for his positivity, critical advice, and hard questions; my friends, for their constancy, love, and eccentricity; and finally my family, for bringing me into this world and raising me to appreciate it.

# Contents

|   |            |
|---|------------|
| <b>Abstract</b>   | <b>ii</b>  |
| <b>Acknowledgements</b>   | <b>iii</b> |
| <b>1 Introduction</b>   | <b>1</b>   |
| 1.1 Fluorescent biomarkers enable real-time quantification of cytosolic protein oxidation . . . . . | 1          |
| 1.2 Limitations of current pipeline . . . . .   | 2          |
| 1.2.1 Inter-frame movement results in measurement error . . . . .                                   | 2          |
| 1.2.2 Segmentation and centerline estimation may require manual input . . . . .                     | 3          |
| 1.3 Aims . . . . .  | 3          |
| <b>2 Methods</b>  | <b>6</b>   |
| 2.1 Edge information helps to differentiate the pharynx from the intestine . . . . .                | 6          |
| 2.2 Flexible measurement boundaries account for anterior-posterior movement . . . . .               | 7          |
| 2.3 Midlines . . . . .  | 8          |
| 2.3.1 A transmitted light image helps to anchor the midlines . . . . .                              | 8          |
| 2.3.2 Dorsoventral tip movement is addressed with frame-specific midlines . . . . .                 | 9          |
| 2.4 Channel Registration picks up the slack . . . . .   | 9          |
| <b>3 Results</b>  | <b>11</b>  |
| 3.1 Definition of error . . . . .   | 11         |
| 3.2 Collection of test data and baseline error quantification . . . . .                             | 11         |
| 3.3 The new analysis pipeline reduces error . . . . .   | 12         |
| <b>4 Discussion</b>   | <b>14</b>  |
| 4.1 Future Directions . . . . .   | 14         |
| 4.1.1 Automatic movement detection . . . . .  | 14         |
| 4.1.2 Extension to different tissues . . . . .  | 14         |
| <b>Bibliography</b>   | <b>16</b>  |

# List of Figures

|     |   |    |
|-----|---|----|
| 1.1 | Ratios of images to reduction potential . . . . .         | 2  |
| 1.2 | Pharyngeal contractions lead to boundary issues . . . . . | 2  |
| 1.3 | Difference images reveal movement . . . . .               | 4  |
| 1.4 | Segmentation of a fluorescence image . . . . .            | 4  |
| 1.5 | The problem with static thresholding . . . . .            | 5  |
| 2.1 | Overview of the improved segmentation algorithm . . . . . | 6  |
| 2.2 | Segmentation of a transmitted-light image . . . . .       | 7  |
| 2.3 | Flexible measurement boundaries . . . . .                 | 7  |
| 2.4 | Previous centerline estimation algorithm . . . . .        | 8  |
| 2.5 | Improved centerline estimation algorithm . . . . .        | 9  |
| 2.6 | Frame-specific midlines . . . . .                         | 9  |
| 2.7 | Functional registration of intensity profiles . . . . .   | 10 |
| 2.8 | Smooth vs. rough functionalization . . . . .              | 10 |
| 3.1 | Errors in old pipeline . . . . .                          | 11 |
| 3.2 | Error by strategy in the synthetic data set . . . . .     | 12 |

# 1 Introduction

Oxidation and reduction (redox) reactions play a vital role in biology. These reactions are characterized by a flow of electrons between chemical species. The species gaining electrons is said to have been oxidized, while the species losing electrons is said to have been reduced. Redox reactions are well-known to be involved in cellular respiration and metabolism more generally. More recently, redox control of the proteome has been the subject of great interest, mediating such events as differentiation and apoptosis [1]. The oxidation of cysteine thiols to disulfide bonds provides an interface between redox chemistry and proteomic signal transduction [2].

Many chemical species in the cell may exist in either an oxidized or reduced form. These pairs, termed *redox couples* facilitate electron transfer in a variety of cellular processes. The NADH/NAD<sup>+</sup> couple, for example, transfers high energy electrons wrought from the oxidation of sugars in the citric acid cycle to O<sub>2</sub> via oxidative phosphorylation.

The healthy cell actively maintains a steady-state disequilibrium of each of these redox couples. The "redox hypothesis" attributes aging and age-related disease to the misregulation of this network [3]. Quantifying redox chemistry in live cells will allow for a deeper understanding of the regulatory mechanisms that mediate these vital processes.

## 1.1 Fluorescent biomarkers enable real-time quantification of cytosolic protein oxidation

In a previous paper, our lab demonstrated the use of the genetically-encoded redox-sensitive fluorescent protein roGFP1\_R12 to quantify the cytosolic reduction potential in the pharyngeal muscle of *C. elegans* in real-time [4]. These redox biosensors are leading to quantitative and mathematical models of the genetics and dynamics of intracellular and organismal-level redox signaling.

A key feature of the roGFP family of sensors is their ratiometric nature, which corrects for differential expression of the sensor, as well as cell thickness [5]. Because the oxidized and reduced form of the protein have differing emission spectra, the emission intensity at differing excitation wavelengths may be used as estimates of concentration in the Nernst equation to determine the sensor's reduction potential [2]. Thanks to the transparent nature of *C. elegans*, fluorescence micrographs reveal spatial reduction potentials at subcellular resolution (Figure 1.1).

Due to the cellular architecture of the pharynx, almost all of the variation in reduction potential follows the posterior-anterior axis. Thus, we can model the pharynx 1-dimensionally as the reduction potential along its posterior-anterior axis without losing significant information. Computationally, this is achieved by (1) estimating the centerline of the pharynx then (2) measuring the intensity of the images under this estimated centerline.

As will be discussed, a fundamental limitation of this analysis arises when the animal moves in the time between capturing the first and second frame in the pair of images required for each animal.

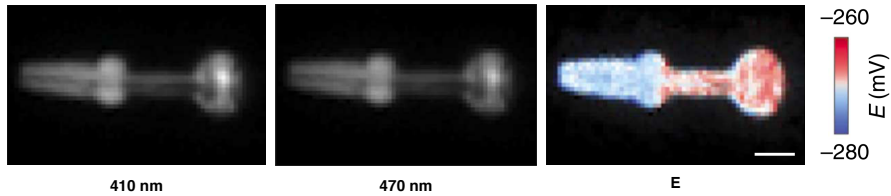


FIGURE 1.1: Pixel-by-pixel ratios are transformed into redox potentials revealing a spatial pattern, adapted from [4]

## 1.2 Limitations of current pipeline

### 1.2.1 Inter-frame movement results in measurement error

The pharynx of *C. elegans* acts as the animal's feeding muscle. It contracts along its anterior-posterior axis, functioning as a pump to bring in food. This contraction poses a problem for ratiometric analysis. Ordinarily, dividing intensities pixel-by-pixel is appropriate because pixel-coordinates in both images capture the same point in physical space. If the animal moves, however, the same point in space is represented by different pixel coordinates in the first and second image. To understand why, consider Figure 1.2.

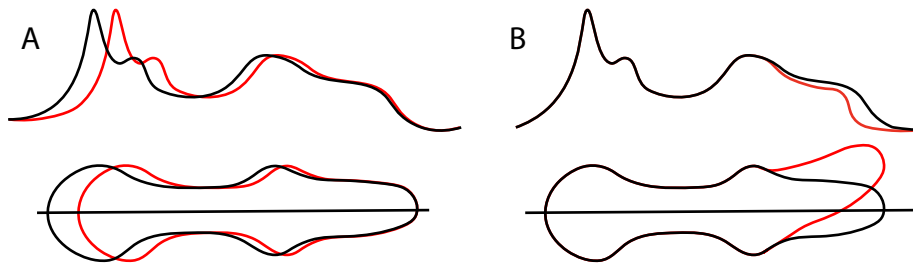


FIGURE 1.2: A cartoon shows the two most common modes of inter-frame movement. **A** Posterior bulb contractions lead to a shrink or stretch of the intensity profile. **B** Dorsal-ventral movement of the anterior tip leads to premature truncation of the intensity profile as the centerline does not follow the curve.

On the bottom we see the outline of the pharynx in each frame. The pharynx has contracted in one frame (red) and is elongated in the other (black). When the intensities along the posterior-anterior axis are plotted above, it is apparent that the contraction has led to unwanted compression of the intensity profile.

Another common mode of inter-frame movement, dorsoventrally at the anterior tip, is represented similarly in Figure 1.2. Dorsoventral anterior tip movements result in a loss of information about the tip in one frame, as depicted in red.

During imaging, animals are paralyzed with the acetyl choline agonist levamisole. However, complete paralysis is not currently possible. Inter-frame movement is currently addressed by visually screening the ratio images for a highly textured appearance, as shown in Figure 1.3. These animals are then excluded from analysis. However, visual screening is a time-intensive process, requires training, and is subject to experimenter error and bias.

### 1.2.2 Segmentation and centerline estimation may require manual input

As noted, the visual screen for inter-frame movement is a manual step. Two other processes in the current pipeline also require manual supervision. The first is segmentation. Segmentation is the process by which pixels corresponding to objects in an image are given salient labels. In this case, the task is to separate the pharynx from everything else (Figure 1.4).

Because the transgenic animals express roGFP with pharynx-specific promoters, most fluorescence occurs only in the region of interest. However, the intestine of *C. elegans* exhibits autofluorescence in response to the wavelengths of light required for roGFP excitation. This poses a problem for the static thresholding algorithm currently used to segment the pharynx. This algorithm assigns any value greater than a threshold the value 1 and those below the threshold 0. Static thresholds work well when the distribution of brightness is different for each class of object in the image, but this is not the case when the intestine autofluoresces, resulting in ill-formed segmentation masks (Figure 1.5).

As described in 1.1, the 1-dimensional model of the pharynx requires the accurate estimation of the tissue's centerline. While the current centerline estimation algorithm (described in 2.3) works well in the interior regions of the pharynx, it is unstable around the terminal regions, both the anterior and posterior. These portions of the centerline must be visually inspected and corrected as well.

## 1.3 Aims

This thesis aims to address the limitations of the current analysis pipeline described in 1.2.1 and 1.2.2. To achieve this, a new pipeline was written in MATLAB to process and analyze these images end-to-end with little to no necessary manual input. The improved pipeline decreases the time required to analyze this data, standardizes the analysis, reduces human error, and mitigates movement-induced error.

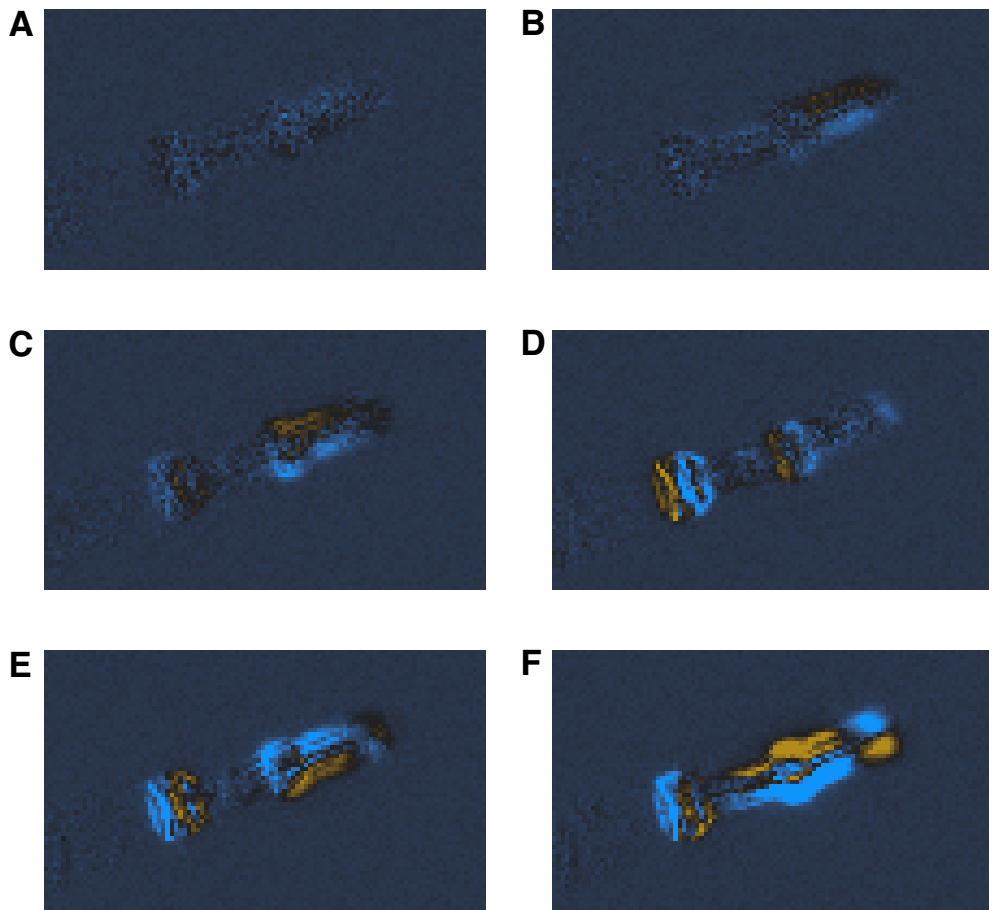


FIGURE 1.3: Signed difference images reveal inter-frame movement. Each image depicts the signed difference between the first and second image in a pair taken at  $\lambda = 410$  nm, colored using a perceptually-uniform diverging colormap, CET-D6 [6]. **A** a pair with minimal inter-frame movement. This pair is considered ideal. **B** a pair with a small amount of dorsoventral around the anterior tip. **C** a pair with a moderate amount of dorsoventral anterior movement **D** a pair with a substantial shift along the posterior-anterior axis. **E** a pair with substantial contractions in the posterior bulb and dorsoventral anterior movement. **F** a pair with substantial contractions in the posterior bulb and dramatic anterior movement

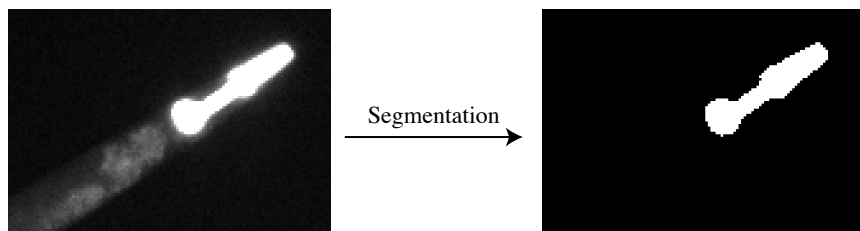
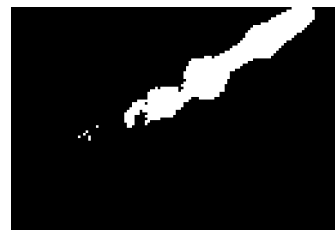


FIGURE 1.4: The goal of segmentation. On the left, the original image showing fluorescence of roGFP in the pharynx and autofluorescence in the gut. On the right, a binary image consisting of value 1 in the pixels with a pharynx and value 0 elsewhere.



---

FIGURE 1.5: The problem with static thresholding. Autofluorescent intestinal tissue results in a segmentation mask that must be manually corrected.

## 2 Methods

### 2.1 Edge information helps to differentiate the pharynx from the intestine

As described in 1.2.2, intestinal autofluorescence causes the static thresholding algorithm to perform insufficiently in separating the pharynx from the rest of the animal and the background. Histogram-based threshold selection algorithms such as Otsu's method also perform poorly when the histograms are not bimodal, as is the case with bright intestinal autofluorescence.

To address these issues, a new segmentation algorithm was developed. This algorithm exploits *edges*, sharp changes in brightness which are information-rich regions in images. The Sobel-Feldman operator creates an image emphasizing edges by discretely differentiating the image in the vertical and horizontal directions (Figure 2.1). By thresholding the resultant image, using morphological operations to remove noise, and selecting the largest region, we isolate the pharynx from gut autofluorescence.

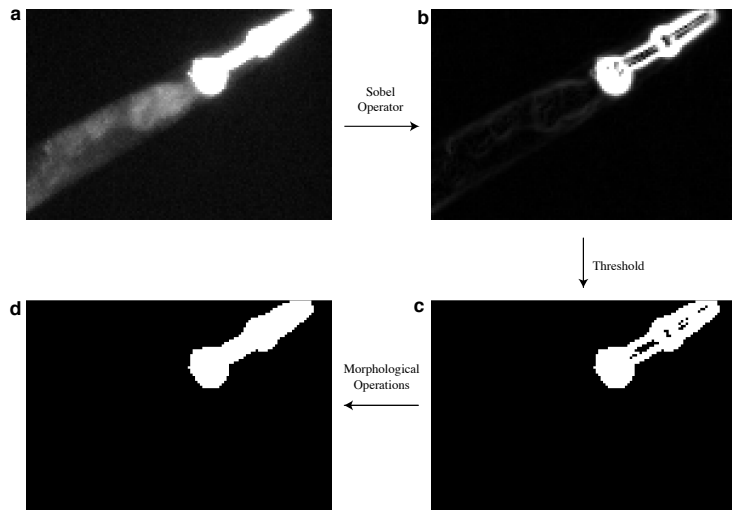


FIGURE 2.1: An overview of the improved segmentation algorithm. **a** The original image, displaying fluorescence of roGFP in the pharynx and the autofluorescence of the gut. **b** The resultant image after application of the sobel operator. **c** The resultant binary image after thresholding the edge-emphasized image. **d** The final segmented binary image, after performing morphological cleaning operations.

For reasons described in 2.3.1, an image taken with transmitted light must also be segmented. Even though the distribution of intensities in transmitted light images are very different from fluorescence images, this edge-based segmentation algorithm still performs robustly (Figure 2.2). This highlights another benefit of the improved method: image brightness independence. If one strain's pharynx fluoresces dimly,

an edge-based segmentation method still performs well while the static thresholding method requires the manual change of the threshold parameter.

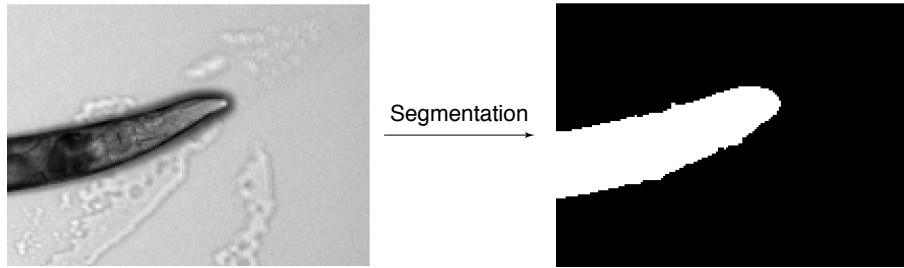


FIGURE 2.2: Segmentation of a transmitted-light image

## 2.2 Flexible measurement boundaries account for anterior-posterior movement

As described in 1.2, inter-frame movement is a large source of error. To understand why, consider the how the previous pipeline takes measurements. First, a single mask using the image taken at 410 nm is computed. This mask is then applied to both the 410 nm and 470 nm images. Pixels corresponding to 1 in the mask retain their value while pixels corresponding to 0 in the mask are assigned the value 0. Measurements are taken of the masked images. Thus, if the animal pumps, measurement might start in the gut or halfway through the posterior bulb, depending on if the animal contracted during the first or second frame. If the animal contracts during the first frame and extends in the second, the mask will be too "short" and measurement in the second frame will start in the middle of the posterior bulb. If the animal is extended in the first frame and contracts in the second, the mask will be too "long" and measurement in the second frame will start in the gut. This error is accounted for via visual inspection of ratio images so as to exclude those animals who have moved from analysis.

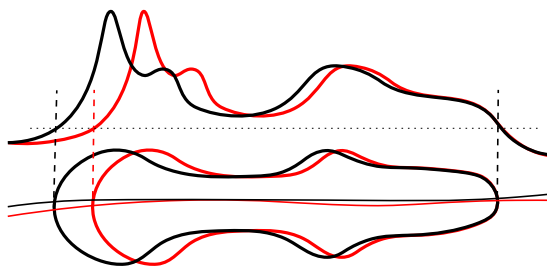


FIGURE 2.3: A cartoon depicting the flexible measurement boundaries in the revised measurement pipeline. The first frame is depicted in black while the second is in red.

The new approach (summarized graphically in Figure 2.3) tries to account for this movement without the need for manual exclusion. Here, segmentation masks are not applied to the images before measurement as before. Instead, they are used only in the calculation of the midlines (described in 2.3). Intensity profiles of the unmasked images are taken under the midlines. The intensity profiles are trimmed to the point where they cross a threshold then resized to the same length via linear

interpolation. Allowing measurement boundaries to move flexibly is a simple yet effective change in reducing error introduced by inter-frame pharyngeal contractions.

## 2.3 Midlines

The previous centerline estimation algorithm takes as input an image of the segmented pharynx aligned horizontally along its anterior posterior axis and works as follows (depicted in figure 2.4).

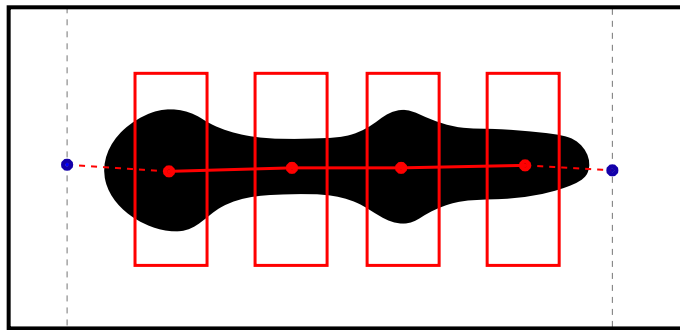


FIGURE 2.4: Cartoon representation of the previous centerline estimation algorithm.

Boxes are drawn at specific static coordinates. The centroid of each shape is calculated (red points). Lines (solid) connect these points. The y-coordinates of the terminating points (blue) are determined via the point-slope method  $y = mx + b$  where  $m$  is the inverse of the slope of the neighboring line,  $x$  is a fixed constant and  $b$  is the y-coordinate of the neighboring point.

### 2.3.1 A transmitted light image helps to anchor the midlines

A major problem faced by the current centerline estimation algorithm is instability around the posterior bulb. Small positional changes in the neighboring points cause the terminal point to move dramatically. These instabilities must be manually corrected.

To address this concern, the new centerline estimation algorithm differs from the old in two ways. First, the new midline is estimated by treating the binary mask as points in coordinate space and fitting them with a B-spline. Second, the new midline incorporates positional information from a transmitted-light image. The algorithm is depicted graphically in Figure 2.5. We segment both the transmitted-light and fluorescence images with the algorithm described in 2.1, resulting in two binary masks. These masks are combined by cutting off the transmitted-light mask when the fluorescence mask starts. The combined mask is fed into the B-spline fit. The points from the transmitted-light mask serve to constrain and anchor the previously unstable posterior-bulb region of the estimated centerline. An additional benefit is that the estimated centerline is defined functionally, and is subject to functional analysis.

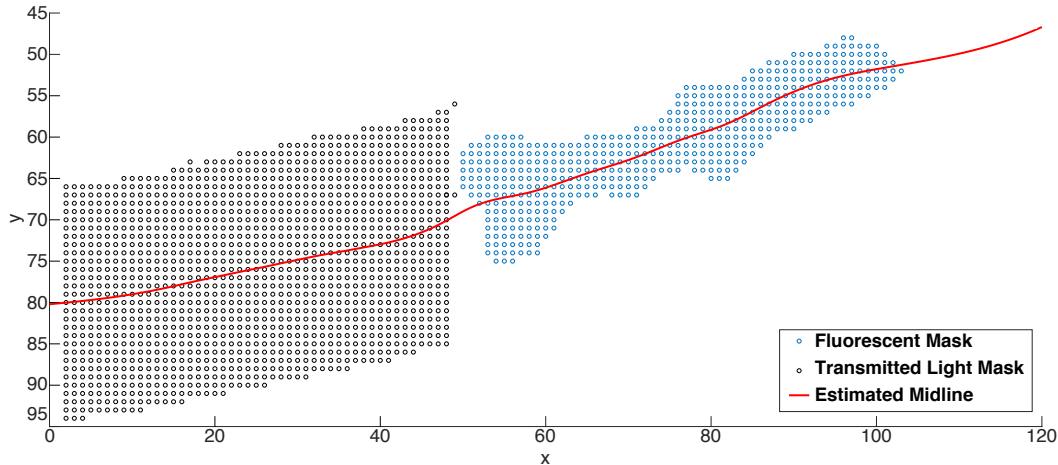


FIGURE 2.5: Depiction of the improved centerline estimation algorithm. Black points correspond to the segmented transmitted-light image, blue points correspond to the segmented fluorescence image.

The estimated midline is shown in red.

### 2.3.2 Dorsoventral tip movement is addressed with frame-specific midlines

We saw in 2.2 a strategy to combat the major mode of inter-frame movement, contractions of the posterior bulb. However, there is another less common mode: dorsal-ventral movement of the tip. The spline algorithm described above allows the centerline to follow the curve of the tip without human intervention. To address inter-frame movement, the new pipeline draws a midline independently in each frame.

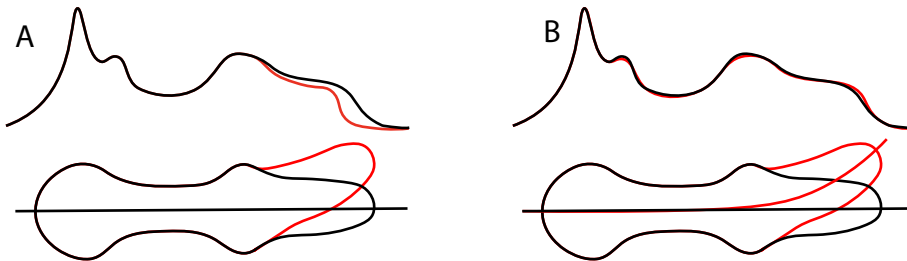


FIGURE 2.6: The result of using frame-specific midlines. **A** Using a single midline ignores the pharynx's curve in the second frame (red), resulting in error in the intensity profile. **B** Frame-specific midlines follow the curve of each shape, resulting in more accurate intensity profiles.

## 2.4 Channel Registration picks up the slack

The frame-specific midline approach discussed in 2.3.2 introduces problems of its own. Specifically, the length of the intensity profile may be dilated nonlinearly due to differences in the arc length of each midline. That is, some sections of the intensity profile measured under these lines might be stretched while others are compressed. To address these nonlinear dilations, we utilized functional registration.

The goal of functional registration is to, given several curves with similar shapes, *register* the curves such that salient features are aligned, but amplitude information from the original curves is unchanged. The algorithms generate a "warping function"  $x_{new} = h(x)$  which maps  $x$  positions along each curve to each other. Figure 2.7 depicts this process.



FIGURE 2.7: A visual representation of the goal of registration. The curves in **A** are unregistered, and contain minimal amplitude variation but significant phase variation. After registration (**B**), the curves retain amplitude variation but phase variation has been removed.

Our pipeline uses the MATLAB package fdaM to perform functional registration. Discrete observations are *functionalized* before registration takes place. Observations were functionalized by fitting a B-spline to the discrete intensity profile. The number of knots for the spline was chosen manually, and a roughness penalty was computed using the generalized cross-validation method. One of the desirable properties of B-spline fitting is that it smooths out noise. However, we aimed to understand how registration contributes to error reduction independently of spline smoothing.

To disentangle the effects of these operations, we register highly smoothed data to obtain a warp function, then apply that warp function to a "rough" fit of the data (Figure 2.8). The error is computed between the resultant warped "rough" functions.

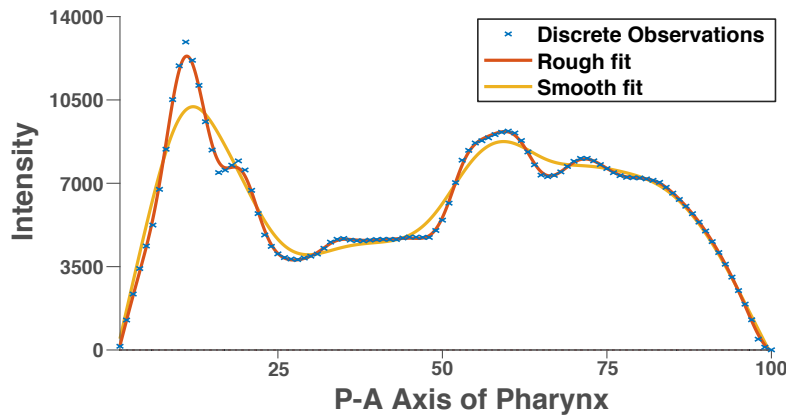


FIGURE 2.8: Discrete observations (blue) are fit with different roughness penalties:  $\lambda = 6.3$  (red),  $\lambda = 100$  (yellow).

# 3 Results

## 3.1 Definition of error

To assess the degree to which changes in the analysis pipeline affect the quality of measurement, a definition of error must first be decided upon. Because intensity varies so dramatically across the pharynx, we are interested in the amount of error *relative* to the intensity at a particular location. Percent error ( $\epsilon$ ) is defined to be a function over pharynx space ( $p$ ) which is the difference between the intensity ( $I$ ) measured in one frame and another, normalized by the average intensity of the two frames at a given wavelength, multiplied by 100. Thus, for  $\lambda = 410$  nm, percent error is given by:

$$\epsilon(p) = \frac{|I_{410_1}(p) - I_{410_2}(p)|}{\frac{I_{410_1}(p) + I_{410_2}(p)}{2}} \times 100$$

## 3.2 Collection of test data and baseline error quantification

A large number of technical replicates were collected in order to establish a baseline empirical estimation of error. A single animal was imaged 57 times in pairs of two, both frames at 410 nm. The ratio images were hand-classified according to the degree of movement (see Figure 1.3) in four regions: the posterior bulb, anterior bulb, sides of the tip, and tip. Figure 3.1 shows the average empirical error as a function of pharynx space, using the previous pipeline to estimate midlines and measure pixel intensities. At the boundaries of the pharynx, errors approach 75% of the intensity, while errors are maximally around 10% of the intensity in the interior regions of the pharynx. In animals that move, error tends to be larger, supporting the suggestion that inter-frame movement is a large source of error. Even in animals that do not move, errors can still reach 8% in the interior regions of the pharynx and increase dramatically at the boundaries.

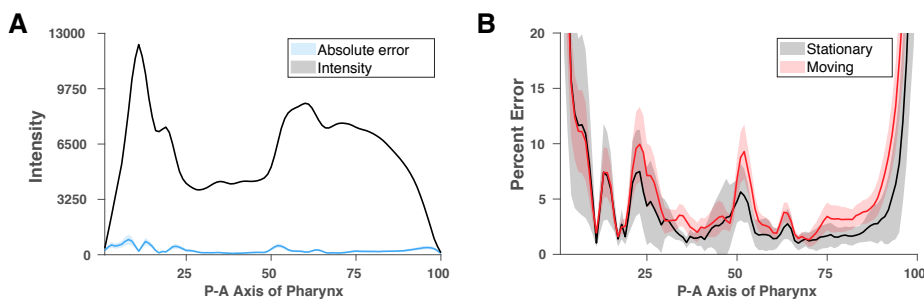


FIGURE 3.1: Baseline quantification of empirical error in test data set. **A** shows the mean intensity (black) profile and absolute error (blue). Absolute error is defined as  $|I_{410_1}(p) - I_{410_2}(p)|$ . **B** shows the percent error in stationary (black) and moving (red) animals.

### 3.3 The new analysis pipeline reduces error

The methods described in this thesis have a substantial effect on measurement error. The combined use of frame-specific masks/midlines and channel registration decreases error from 3-9% to less than 3% across the entire pharynx (Figure 3.2). Notably, the error around the boundaries remains stable when measuring with the new pipeline. The new pipeline decreases error across all regions of the pharynx, even in stationary animals.

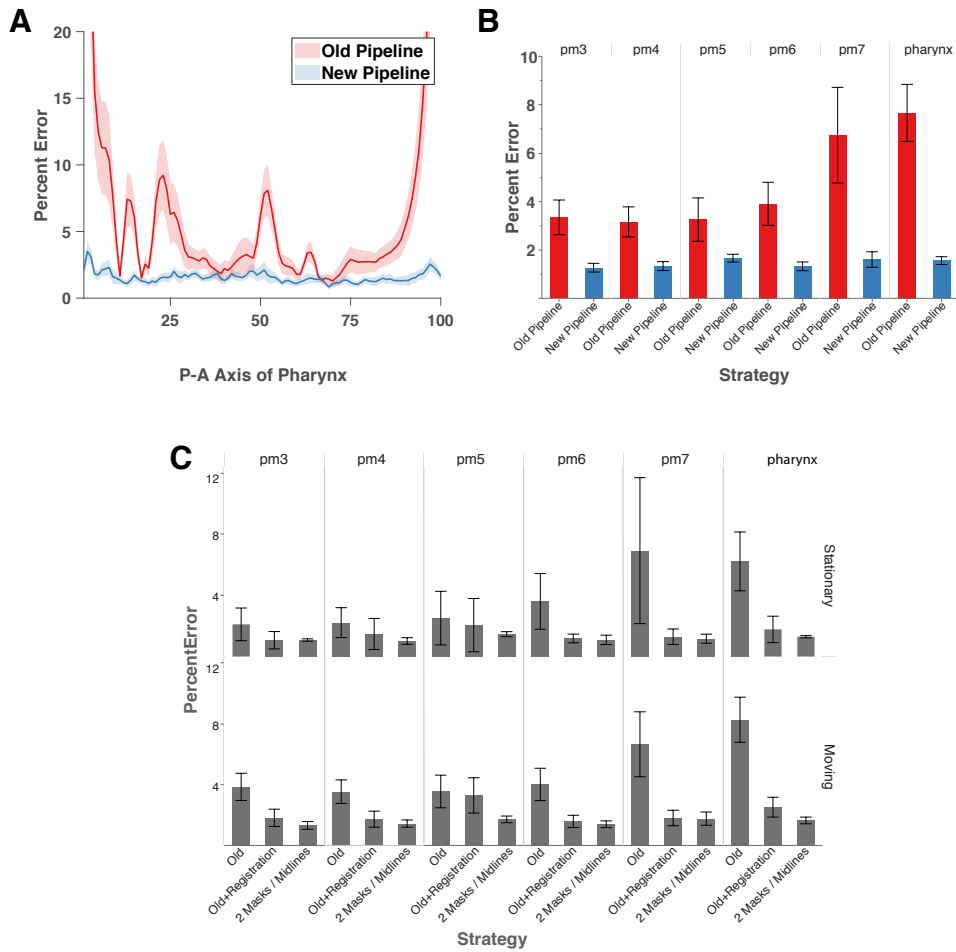


FIGURE 3.2: **A** Percent error is reduced across the entire pharynx space by use of the new pipeline as compared to the old pipeline. **B** Errors are averaged over physiologically relevant boundaries. pm3–pm7 are cells in the pharyngeal muscle ordered sequentially along the posterior-anterior axis; “pharynx” refers to an average over the entire profile. **C** The effect of different strategies on percent error in stationary and moving animals. “Old+registration” applies the functional registration strategy described in 2.4 to the intensity profiles obtained via the old pipeline, while “2 Masks / Midlines” uses the new methodologies for computing frame-specific masks and midlines but forgoes functional registration

Registration and frame-specific masks/midlines seem to act redundantly in reducing error. In effect, the flexible measurement boundaries enabled by frame-specific masks and midlines perform a limited form of registration. Specifically, they can register intensity profiles which need a linear stretch or compression (when the

animal pumps between frames). When the pharynx moves dorsoventrally, the posterior regions of the pharynx remain stationary while the anterior tip of the pharynx moves. While a frame-specific midline can capture this movement, differences in the arc-length of the midline requires the non-linear registration strategy described in 2.4. Dorsoventral movement is relatively rare as compared to pumping, and a larger data set is needed to understand the quantitative reduction in error attributed to this non-linear registration.

# 4 Discussion

Genetically encoded redox-sensitive fluorescent biomarkers have spurred a revolution in the study of dynamic cellular redox processes. While the ratiometric nature of these sensors yields many desirable qualities, it also necessitates careful analysis in the event of inter-frame movement.

This thesis has introduced how inter-frame movement introduces error in ratiometric fluorescent microscopy and proposed three strategies to mitigate this error in the context of the pharyngeal muscle of the nematode *C. elegans*. Frame-specific masks allow for flexible measurement boundaries, which achieves a limited form of global linear registration. Frame-specific midlines account for the dorsoventral movement common at the anterior regions of the pharynx. A functional approach to registration accounts for the differences in arc-length of the frame-specific midlines, and achieves the non-linear registration that frame-specific midlines require. These improvements allow previously unusable data to be re-analyzed and will require fewer animals to be excluded in future experiments.

This thesis has also shown how new approaches to segmentation and centerline estimation reduces the need for manual input in the pipeline via incorporation of edge information and transmitted-light information, respectively. In most cases, the pipeline requires no manual input and analysis can be done with little effort and time, increasing experimental throughput.

## 4.1 Future Directions

### 4.1.1 Automatic movement detection

This thesis has focused on the mitigation of the error introduced by inter-frame movement. As noted, not all error can be removed by these methods. As such, it would be useful for an automated classification system to detect inter-frame movement. The fundamental difficulty with this task is that in an experimental setting the image pairs consist of one image at 410 nm and another at 470 nm. Because the excitation spectra of roGFP is different at each wavelength, it is difficult to determine if the differences in each image's intensity profile is due to movement or true biochemical activity. This concern could be addressed by quantifying distance between midlines instead of difference in intensity profile. Alternatively, different imaging strategies could be developed. For example, if four images were taken of each animal at alternating excitation wavelengths, differences in the pairs with the same wavelength could be used to quantify error and thereby inter-frame movement.

### 4.1.2 Extension to different tissues

The analysis pipeline described in this thesis is highly specific to the pharyngeal muscle. Due to its stereotyped geometry, this tissue has been an ideal foundation on which to build. However, there is considerable interest in understanding dynamic redox processes in other tissues such as the intestine and nervous system. Each tissue will surely introduce its own challenges that will need to be individually

addressed. Precise methodologies for quantifying redox processes in these different tissues will lead to a deeper understanding of how these processes are regulated at an organismal level.

# Bibliography

1. Circu, M. L. & Aw, T. Y. Reactive Oxygen Species, Cellular Redox Systems, and Apoptosis. *Free Radical Biology and Medicine* **48**, 749–762. ISSN: 08915849 (Mar. 15, 2010).
2. Meyer, A. J. & Dick, T. P. Fluorescent Protein-Based Redox Probes. *Antioxid. Redox Signal.* **13**, 621–650 (2010).
3. Jones, D. P. Radical-Free Biology of Oxidative Stress. *Am J. Physiol. Cell Physiol.* **295**, C849–C868 (2008).
4. Romero-Aristizabal, C., Marks, D. S., Fontana, W. & Apfeld, J. Regulated Spatial Organization and Sensitivity of Cytosolic Protein Oxidation in *Caenorhabditis Elegans*. *Nature Communications* **5**. ISSN: 2041-1723. doi:10 . 1038 / ncomms6020. <http://www.nature.com/articles/ncomms6020> (2019) (Dec. 2014).
5. Hanson, G. T. Investigating Mitochondrial Redox Potential with Redox-Sensitive Green Fluorescent Protein Indicators. *J. Biol. Chem.* **279**, 13044–13053 (2004).
6. Kovesi, P. Good Colour Maps: How to Design Them. arXiv: [1509 . 03700 \[cs\]](https://arxiv.org/abs/1509.03700). <http://arxiv.org/abs/1509.03700> (2019) (Sept. 11, 2015).